Acta Crystallographica Section D
Biological Crystallography
ISSN 0907-4449

Structures of the nucleotide-binding domain of the human ABCB6 transporter and its complexes with nucleotides

Matthias Haffke,[a] Anja Menzel,[a] Yvonne Carius,[a] Dieter Jahn[b] and Dirk W. Heinz[a]*

[a]Division of Structural Biology, Helmholtz Zentrum für Infektionsforschung, D-38124 Braunschweig, Germany, and [b]Institute of Microbiology, Technische Universität Braunschweig, D-38106 Braunschweig, Germany

Correspondence e-mail: dirk.heinz@helmholtz-hzi.de

Received 21 June 2010
Accepted 17 July 2010

PDB References: nucleotide-binding domain of human ABCB6 transporter, nucleotide-free, 3nh6; complex with ADP, 3nhb; complex with ADP and Mg^{2+}, 3nha; complex with ATP, 3nh9.

The human ATP-binding cassette (ABC) transporter ABCB6 is involved in haem-precursor transport across the mitochondrial membrane. The crystal structure of its nucleotide-binding domain (NBD) has been determined in the apo form and in complexes with ADP, with ADP and Mg^{2+} and with ATP at high resolution. The overall structure is L-shaped and consists of two lobes, consistent with other reported NBD structures. Nucleotide binding is mediated by the highly conserved Tyr599 and the Walker A motif, and induces notable structural changes. Structural comparison with other structurally characterized NBDs and full-length ABC transporters gives the first insight into the possible catalytic mechanism of ABCB6 and the role of the N-terminal helix α_1 in full-length ABCB6.

1. Introduction

Haem is an important cofactor of many proteins and enzymes. In eukaryotes its biosynthesis begins and ends in the mitochondria and/or chloroplasts, whereas some intermediates are processed in the cytosol. In humans the synthesis of haem starts with the production of δ-aminolevulinic acid (ALA) from succinyl-CoA and glycine in the mitochondria. ALA is then transported across the mitochondrial membrane into the cytosol, where it is cyclized to porphobilinogen. After three more enzymatic reactions, coproporphyrinogen III (CPgenIII) is formed, which has to be translocated back into the mitochondria for further processing. The transport of CPgenIII through the outer mitochondrial membrane is achieved *via* the so-called ABCB6 transporter (Krishnamurthy *et al.*, 2006; Paterson *et al.*, 2007). ABCB6 belongs to the ATP-binding cassette (ABC) superfamily (Higgins, 1992), which is one of the largest protein families. ABC proteins are responsible for the transport of a wide range of endogenous and xenobiotic compounds such as fatty acids, sugars, peptides and antibiotics (Borst & Elferink, 2002; Holland & Blight, 1999). The human ABC-transporter family consists of 49 identified genes (Dean *et al.*, 2001). The ABC transporters can be divided into seven major subfamilies named A–G.

Numerous ABC genes are associated with inherited diseases (Dean *et al.*, 2001) such as Tangier disease T1 (ABCA1), Stargardt diseases (Allikmets *et al.*, 1997), retinitis pigmentosa and age-related macular degeneration (ABCA4), progressive familial intrahepatic cholestasis (ABCB11; de Vree *et al.*, 1998), Dubin–Johnson syndrome (ABCC2; Wada *et al.*, 1998), pseudoxanthoma elasticum (ABCC6; Dean *et al.*, 1990), cystic fibrosis (ABCC7), X-linked adrenoleuko-

dystrophy (ABCD1 and ABCD2), Zellweger syndrome (ABCD3 and ABCD2) and sitosterolaemia (ABCG5 and ABCG8; Berge *et al.*, 2000). Further ABC genes are currently being investigated for potential involvement in certain inherited metabolic diseases.

ABCB6 is a member of ABC subfamily B, which consists of 11 exclusively mammalian genes. As some of these members are involved in multidrug resistance (MDR) in cancer (Szakacs *et al.*, 2004; Sharom, 2008), the ABCB subfamily is called the MDR family of ABC transporters. Furthermore, as human ABCB6 is involved in various diseases such as cancer (Emadi-Konjin *et al.*, 2002) and in the homeostasis of cellular iron and the maturation of iron–sulfur proteins (Kispal *et al.*, 1997, 1999), its dysfunction could be directly linked to a disorder of mitochondrial function.

ABCB6 is a transmembrane protein with 11 predicted transmembrane helices (TMs) arranged in two membrane-spanning domains (MSDs) and a nucleotide-binding domain (NBD), which is located on the cytosolic side of the membrane (Tsuchida *et al.*, 2008). ABCB6 has to dimerize to form a functional unit of four MSDs and two NDBS. Therefore, ABCB6 is called a 'half-size' ABC transporter.

The NBDs of similar transporters from a variety of organisms such as *Homo sapiens*, *Mus musculus*, *Rattus norvegicus*, *Escherichia coli*, *Salmonella typhimurium* and *Methanococcus janaschii* have been structurally characterized (see Supplementary Table 1[1]). However, only recently has the structure of a eukaryotic full-length transporter, ABCB1 from *M. musculus*, been reported (PDB entry 3g5u; Aller *et al.*, 2009). The structures of the NBDs from the ABC superfamily contain as characteristic features the widely conserved Walker A, Walker B, Q-loop, P-loop, A-loop and ABC signature sequence motifs (Schneider & Hunke, 1998), which are part of the nucleotide-binding site architecture. These motifs harbour the basis of ATP specificity (Higgins, 1992; Holland & Blight, 1999).

In order to gain a structural understanding of human ABCB6, we have initiated the characterization of its NBD. Here, we report the structure determination of the NBD from human ABCB6 in various states: apo and in complexes with ADP, with ATP and with ADP and Mg^{2+}.

Table 1
Data-collection and refinement statistics.

Values in parentheses are for the highest resolution shell.

	Apo ABCB6 NBD	ABCB6 NBD–ADP	ABCB6 NBD–ADP–Mg^{2+}	ABCB6 NBD–ATP
Beamline	ESRF ID14.1	Cu $K\alpha$, Rigaku MicroMax-007 HF	DESY X11	Cu $K\alpha$, Rigaku MicroMax-007 HF
Space group	$P2_12_12_1$	$P2_12_12_1$	$P2_12_12_1$	$P2_12_12_1$
Unit-cell parameters (Å)	a = 57.23, b = 68.61, c = 76.54	a = 56.18, b = 70.81, c = 70.69	a = 56.27, b = 70.71, c = 71.11	a = 57.15, b = 65.63, c = 69.52
Wavelength (Å)	0.93	1.54	0.815	1.54
Resolution (Å)	33.4–2.00 (2.15–2.00)	24.5–2.15 (2.21–2.15)	44.1–2.10 (2.15–2.10)	24.5–2.10 (2.15–2.10)
Measured reflections	317134 (55623)	121632 (5773)	67265 (3480)	56816 (3400)
Unique reflections	20977 (4013)	15793 (1145)	17052 (1125)	15449 (1021)
$\langle I/\sigma(I)\rangle$	37.1 (5.2)	12.3 (3.3)	14.7 (2.4)	15.8 (2.9)
Completeness (%)	99.9 (100)	99.4 (99.2)	99.5 (97.9)	97.7 (90.4)
Redundancy	15.1 (12.2)	7.7 (5.0)	3.9 (3.2)	3.7 (3.3)
R_{merge} (%)	5.8 (62.5)	15.2 (63.0)	6.6 (58.5)	7.0 (47.4)
R_{meas} (%)	6.0 (64.9)	16.3 (70.0)	7.7 (70.7)	8.1 (55.7)
Wilson B factor (Å^2)	32.6	21.4	33.2	25.1
Solvent content (%)	45.2	41.4	41.8	36.8
R_{work} (%)	18.0	18.1	18.4	17.5
R_{free} (%)	23.9	24.3	25.2	24.8
Protein atoms	2152	2142	2119	2112
Solvent atoms	139	142	129	152
R.m.s.d. from ideal geometry				
Bond lengths (Å)	0.017	0.018	0.018	0.019
Bond angles (°)	1.512	1.752	1.619	1.744
Average B factors (Å^2)				
Protein	39.8	24.7	34.8	29.7
Solvent	49.3	32.5	42.6	38.2
Nucleotide	—	18.9	33.2	22.8
Ramachandran plot (%)				
Favoured	98.2	97.5	97.5	98.6
Allowed	1.8	2.5	2.5	1.4

2. Materials and methods

2.1. Cloning, expression and purification

The sequence of the NBD of the human ABCB6 gene, corresponding to amino acids 558–842 of the full-length transporter, was amplified by polymerase chain reaction from pOT7b_abcb6 with forward primer 5′-CATATGTTCATTGACATGGAGAACATGTTTG-3′ and reverse primer 5′-CTCGAGTCACCGTTCCATGGTCTGAG-3′. For expression, the sequence of the NBD was cloned into pET28c (Novagen) *via* *Nde*I and *Xho*I restriction sites by TOPO cloning (Invitrogen) using the pCR-BluntII-TOPO vector (Invitrogen). The finally obtained construct contained a His_6 tag and thrombin cleavage site N-terminal to amino acids 558–842 of the full-length transporter. Therefore, the sequence of the N-terminal region preceding Phe558 is MGSS**HHHHHH**SSG**LVPRGS**HM (the His_6 tag and thrombin cleavage site are shown in bold).

For protein production, transformed Tuner (DE3) cells were used, which showed a slightly higher expression of the desired protein compared with BL21 (DE3) or Rosetta (DE3) cells. The cells were cultured at 310 K to an $OD_{600\,nm}$ of 0.6–0.8 in LB medium containing 1% tryptone, 0.7% NaCl, 0.5% yeast extract and 30 µg ml^{-1} kanamycin. Cells were shifted to

[1] Supplementary material has been deposited in the IUCr electronic archive (Reference: BE5152). Services for accessing this material are described at the back of the journal.

291 K and gene expression was induced with 1 m*M* isopropyl *β*-D-1-thiogalactopyranoside. The cells were grown for an additional 24 h and harvested by centrifugation at 6000*g* at 277 K.

The cells were lysed by sonication in 50 m*M* Tris–HCl pH 7.5 containing 300 m*M* NaCl, 5 m*M* imidazole, 0.1 mg ml^{-1} lysozyme and a Complete EDTA-free protease-inhibitor tablet (Roche). The lysate was centrifuged at 60 000*g* for 60 min at 277 K to remove cell debris. The supernatant was loaded onto a column with 10 ml Ni–NTA Sepharose Superflow resin (Qiagen) equilibrated with 50 m*M* Tris–HCl pH 7.5, 300 m*M* NaCl, 5 m*M* imidazole and washed with ten column volumes of 50 m*M* Tris–HCl pH 7.5, 300 m*M* NaCl, 10 m*M* imidazole.

Bound protein was eluted using an imidazole gradient from 50 to 500 m*M* in 50 m*M* Tris–HCl pH 7.5, 300 m*M* NaCl.

The protein was finally purified by gel filtration using a Superdex 75 16/60 column (GE Healthcare) equilibrated with 50 m*M* Tris–HCl pH 7.5, 150 m*M* NaCl and 5 m*M* 2-mercaptoethanol. Sample fractions were analyzed for purity and polydispersity by SDS–PAGE and dynamic light scattering (DynaPro Titan, Wyatt). Pure and monodisperse fractions were pooled and concentrated to 10 mg ml^{-1} with Vivaspin 10K molecular-weight cutoff concentrators (Sartorius).

2.2. ATPase activity assay

ATPase activity was analyzed using a P_i-detection kit from Innova Biosciences. Briefly, 100 µl reaction mixture consisting of 100 µg protein, 1 m*M* ATP and 5 m*M* $MgCl_2$ in 50 m*M* Tris–HCl pH 7.5, 150 m*M* NaCl was incubated for different periods of time at 293 K. The reaction was stopped by adding the PiColorLock Gold reagent mixture followed by addition of the stabilizer reagent after 5 min. Absorbance was measured after an additional incubation step for 45 min at 635 nm in a microtitre plate (Greiner) in an Infinite M200 reader (Tecan).

2.3. Crystallization

Crystals were grown by the hanging-drop vapour-diffusion method using a mixture of 1 µl protein solution (10 mg ml^{-1} in 50 m*M* Tris–HCl pH 7.5, 150 m*M* NaCl, 5 m*M* 2-mercaptoethanol) and 1 µl reservoir solution consisting of 40%(*v*/*v*) PEG 400 in 0.1 *M* MES pH 6.5. The protein–reservoir mixture was equilibrated against 500 µl reservoir solution. Cocrystallized structures were obtained using similar crystallization conditions with 3 m*M* ADP or with 3 m*M* ADP and 3 m*M* $MgCl_2$. Initial crystals grew at 292 K overnight and reached final size within one week. ATP-bound ABCB6 NBD was obtained by soaking nucleotide-free crystals in a 2 µl drop of 40%(*v*/*v*) PEG 400 and 30 m*M* ATP in 0.1 *M* MES pH 6.5 at 292 K for 1 h.

2.4. Data collection, processing and structure determination

Crystals were flash-cooled in liquid nitrogen and X-ray diffraction data were collected at 100 K on beamline ID14.1 at ESRF (Grenoble, France) equipped with an ADSC Q210 CCD detector, on beamline X11 at DESY (Hamburg, Germany) equipped with a MAR 555 flat-panel detector or using a MicroMax-007 HF rotating copper-anode X-ray generator (Rigaku) with a Saturn 944+ CCD detector (Rigaku).

Data were processed with *XDS*/*XSCALE* (Kabsch, 2010). The free *R* factor (R_{free}) was calculated from 5% of randomly chosen reflections. Matthews coefficient (Matthews, 1968) calculations indicated one monomer per asymmetric unit (V_M = 2.20 Å^3 Da^{-1}). The apo structure of the NBD of the human ABCB6 transporter was solved by molecular replacement (MR) with *MOLREP* (Vagin & Teplyakov, 2000) using the structure of multidrug-resistance protein 2 (MDRP2) from *Plasmodium yoelii* (PDB entry 2ghi; 47% sequence identity to ABCB6 NBD; Vedadi *et al.*, 2007) as a search model. One solution with an initial *R* value of 0.53 was obtained. The *R* value decreased to 0.40 after 30 cycles of

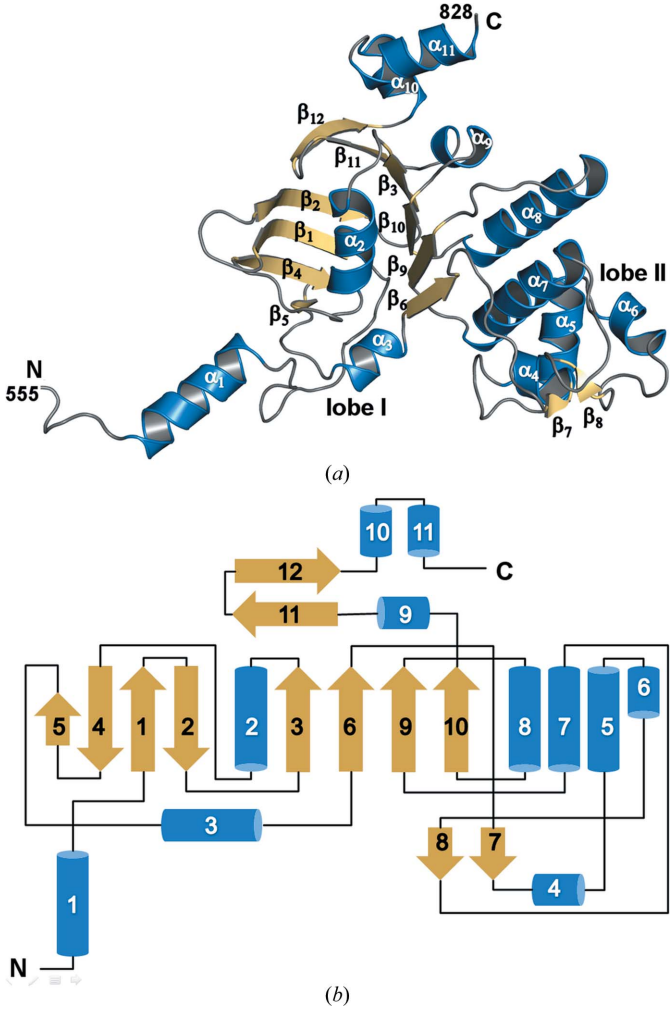

Figure 1
Overall structure of the NBD of ABCB6. *α*-Helices are coloured blue and *β*-strands are coloured yellow. The N- and C-termini are indicated by capital letters. (*a*) The overall L-shaped structure of ABCB6 NDB is formed by two lobes. The ABC core subdomain and the ABC *β* antiparallel subdomain together form lobe I, whereas lobe II consists of the ABC *α* subdomain. Helix α_1 protrudes to the left in this figure. The figure was prepared with *PyMOL* (DeLano, 2008). (*b*) Topology plot of ABCB6 NBD. The central helix α_2 is surrounded by a parallel *β*-sheet (β_3, β_6, β_9, β_{10}, β_{11} and β_{12}) and an antiparallel *β*-sheet (β_1, β_2, β_4 and β_5).

restrained refinement in *REFMAC*5 (Murshudov *et al.*, 1997). An initial model of the NBD of human ABCB6 was built using *ARP*/*wARP* (Lamzin & Wilson, 1993), which decreased the R_{work} value to 0.22. Further model building was performed with *Coot* (Emsley *et al.*, 2010) and water molecules were added by *ARP*/*wARP* (Langer *et al.*, 2008) into peaks higher than 3.5σ in the $F_o - F_c$ map. Water molecules were finally checked for hydrogen bonding in *Coot* and modified if necessary. Additional rounds of restrained refinement including a final TLS refinement (Painter & Merritt, 2006*a*) step using four TLS groups as determined by the *TLS Determination Server* (Painter & Merritt, 2006*b*) were carried out with *REFMAC*5. The final *R* values were R_{work} = 18.0% and R_{free} = 23.9%.

Structures of the ADP-bound, the ADP- and Mg^{2+}-bound and the ATP-bound forms of ABCB6 NBD were similarly solved using the refined apo structure as a search model for MR. Data-collection and refinement statistics are listed in Table 1. The final models were checked and validated using *WHAT IF* (Vriend, 1990) and *PROCHECK* (Laskowski *et al.*, 1993), which indicated good-quality models. All residues were within allowed regions of the Ramachandran plot (Ramachandran & Sasisekharan, 1968).

The atomic coordinates and the structure factors for all four structures have been deposited in the Protein Data Bank (Bernstein *et al.*, 1977) under accession codes 3nh6 (nucleotide-free), 3nhb (complex with ADP), 3nha (complex with ADP and Mg^{2+}) and 3nh9 (complex with ATP).

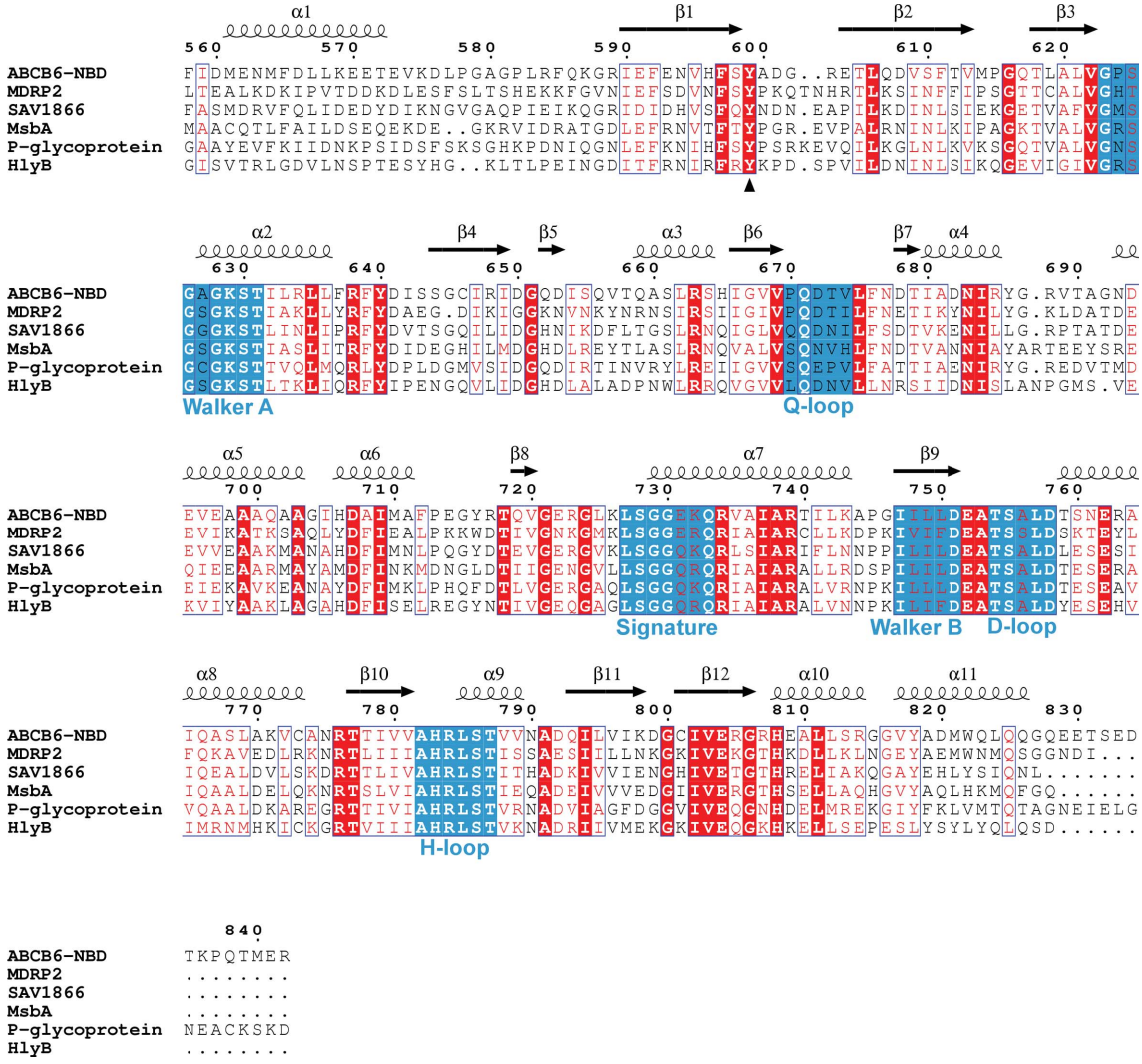

Figure 2
Sequence alignment of ABCB6 NBD with the five full-length ABC transporters MDRP2 (*Plasmodium yoelii*; PDB entry 2ghi; NBD only), SAV1866 (*Staphylococcus aureus*; PDB entry 2onj; full-length transporter), MsbA (*Salmonella typhimurium*; PDB entry 3b60; full-length transporter), P-glycoprotein (*Mus musculus*; PDB entry 3g5u; full-length transporter) and HlyB (*Escherichia coli*; PDB entry 3b5j; NBD only), the structures or NBD structures of which showed the highest *Z* scores and lowest r.m.s.d.s according to the *DALI* server (Holm, 1998). The sequence alignment was scaled down to the NBD of ABCB6 as investigated in the present study. Conserved motifs among NBDs are highlighted in blue and labelled below the sequence alignment. The secondary structures at the top of the sequence alignment correspond to the structure of ABCB6 NBD determined in the present study and were assigned with *DSSP* (Kabsch & Sander, 1983). The highly conserved tyrosine, which is important for nucleotide binding, is indicated by a black triangle. Fully conserved residues are coloured white on a red background; partially conserved residues are coloured red on white background. Sequences were aligned with *ClustalW*2 (Larkin *et al.*, 2007) and the alignment was edited with *ESPript* (Gouet *et al.*, 1999).

3. Results and discussion

3.1. ATPase activity assay

The ATPase activity assay (Supplementary Fig. S1) showed that the isolated and purified NBD of ABCB6 retained its enzymatic activity. Activity was only observed in the presence of Mg^{2+}. Analytical gel filtration in the presence of ATP or of AMPPNP (5′-adenylyl-β,γ-imidodiphosphate), a nonhydrolysable ATP analogue, did not indicate nucleotide-dependent dimerization of ABCB6 NBD (data not shown), in contrast to the findings for other isolated NBDs (Guo *et al.*, 2006; Zaitseva, Jenewein, Jumpertz *et al.*, 2005).

3.2. Overall structure

His_6-ABCB6 NBD crystallized with one monomer per asymmetric unit in the nucleotide-free form as well as in the ADP- and the ADP- and Mg^{2+}-bound forms. The ATP-bound form was obtained by soaking nucleotide-free crystals and also contained one monomer per asymmetric unit. Several trials of cocrystallization with ATP or AMPPNP did not yield diffracting crystals.

All models of the NBD of ABCB6 included the N-terminal region at least up to Phe558, the first amino acid of the NBD of ABCB6 as chosen for structural studies. However, part of the N-terminus covering the N-terminal His_6 tag and the thrombin cleavage site could not be located within the electron-density map ($2F_o - F_c$) for all four structures. A flexible region (amino acids Lys569–Glu573) connecting helix α_1 to lobe I in the ADP and the ADP and Mg^{2+} cocrystallized structures was poorly defined in the electron density. The same was found for part of the A-loop in the ADP and the ADP and Mg^{2+} cocrystallized ABCB6 NBD, in which the side chains of residues Asp601–Arg603 could not be located clearly within the $2F_o - F_c$ map and were therefore modelled as alanines or completely omitted (Gly602). The C-terminal regions could be built up to Gly827 in all structures.

The largest crystal contact area between two monomers (correlating symmetry operation $-x - \frac{1}{2}, -y, z - \frac{1}{2}$) was calculated as 870 Å^2 between helix α_1 (monomer 1) and α_9, α_{10}, α_{11}, β_{11} and β_{12} (monomer 2) according to the *PISA* server (Krissinel & Henrick, 2007) and does not represent a physiological interaction.

The overall structure of ABCB6 is roughly L-shaped (Fig. 1*a*) and is formed by two lobes with overall dimensions of about 50 × 55 × 30 Å (without the N-terminal helix α_1). Lobe I contains the so-called ABC core subdomain (Karpowich *et al.*, 2001), which is formed by a parallel β-sheet consisting of β-strands β_3, β_6, β_9, β_{10}, β_{11} and β_{12} and its flanking α-helices α_2, α_3, α_8, α_9, α_{10} and α_{11}. The antiparallel β-sheet within lobe I consisting of β_1, β_2, β_4 and β_5 is designated the ABC β antiparallel subdomain (Jones & George, 2007). The ABC α subdomain, which is built by helices α_4, α_5, α_6 and α_7, forms lobe II. The otherwise globular structure is extended by the 16 Å long N-terminal helix α_1, which clearly protrudes from both lobes (Fig. 1*a*). This N-terminal helix connects the NBD of ABCB6 with its TMDs as suggested by comparison with the structure of full-length murine P-glycoprotein (PDB entry 3g5u; Aller *et al.*, 2009; Fig. 6).

A comparison with NBDs from other ABC transporters reveals high similarities in sequence (Fig. 2) and structure, with r.m.s.d.s of 1.7 Å for that from *Staphylococcus aureus* (PDB entry 2onj; full-length transporter; SAV1866), 1.5 Å for that from *P. yoelii* (PDB entry 2ghi; NBD only; MDRP2), 1.5 Å for that from *Mus musculus* (PDB entry 3g5u; full-length transporter; P-glycoprotein), 2.0 Å for that from *Salmonella typhimurium* (PDB entry 3b60; full-length transporter; MsbA) and 1.9 Å for that from *E. coli* (PDB entry 3b5j; NBD only; HlyB) as calculated by secondary-structure matching in *CCP*4*MG* (Potterton *et al.*, 2004).

The overall structure of ABCB6 NBD in complex with nucleotides shows a number of structural changes when compared with the apo structure (Fig. 3). Lobe II rotates inwards with respect to lobe I, as also observed for other isolated NBDs (Zaitseva, Jenewein, Wiedenmann *et al.*, 2005). The r.m.s.d. for lobe II (using lobe I without helix α_1 as a fitting region in *ProFit*; Martin, 2009) was calculated as 1.49, 1.42 and 1.28 Å for the ATP, the ADP and the ADP and Mg^{2+} complexes, respectively. Furthermore, helix α_1 is distorted and shortened by one turn in the ADP and the ADP and Mg^{2+} complex structures. However, this is not the case for the ATP complex structure, which was obtained by soaking in contrast to the cocrystallized ADP and the ADP and Mg^{2+} complexes. These differences indicate that the loop connecting helix α_1 to lobe I is highly flexible and might represent a hinge region in full-length ABCB6 (Fig. 6). Helix α_2 is tilted towards the ABC β antiparallel subdomain and the conformation of the Walker A motif at the N-terminal region of α_2 is also changed (Fig. 3). The changes in the overall structure upon nucleotide binding and the differences between the ATP, the ADP and the ADP and Mg^{2+}

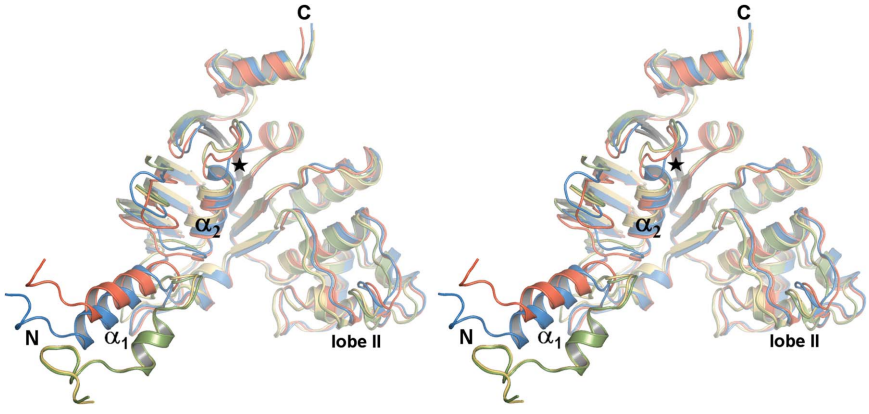

Figure 3
Structural changes within ABCB6 NBD induced by nucleotide binding. Nucleotide-free ABCB6 NBD is coloured blue, whereas the ATP complex is coloured red, the ADP complex is coloured yellow and the ADP and Mg^{2+} complex is coloured green. The Walker A motif at the N-terminus of helix α_2 is marked by a black asterisk. This stereo figure was prepared with *PyMOL* (DeLano, 2008).

complex structures indicate that ATP hydrolysis is coupled with intramolecular movements. Such structural changes are necessary for the transport process of ABC transporters that allows the shuttling of substrates across the membrane (Dawson *et al.*, 2007; Higgins & Linton, 2004; Hollenstein *et al.*, 2007).

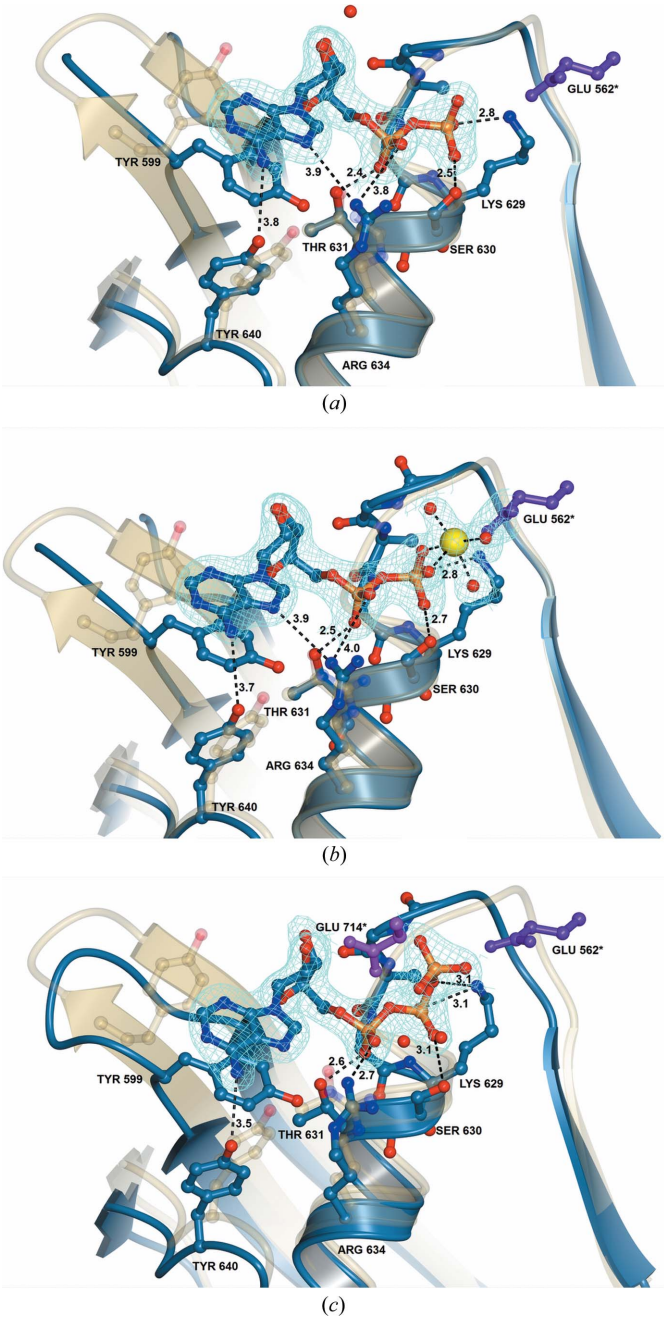

(*a*)

(*b*)

(*c*)

Figure 4
Nucleotide binding to ABCB6 NBD. Nucleotide-bound ABCB6 NBD is colored blue and apo ABCB6 NBD is coloured yellow. The electron density ($2F_o - F_c$) is contoured at 1σ. Hydrogen bonds are shown for the indicated side chains only. Water molecules bridging the nucleotide and the protein are shown as red spheres. Crystal contacts interacting with the nucleotide are shown in dark purple or purple and are marked by an asterisk. (*a*) Complex with ADP. (*b*) Complex with ADP and Mg^{2+} (yellow sphere). (*c*) Complex with ATP. These figures were prepared with *CCP4MG* (Potterton *et al.*, 2004).

3.3. Nucleotide binding

The detailed view of the nucleotide-binding site of ABCB6 NBD reveals important residues that are involved in nucleotide binding (Fig. 4). All nucleotides could be located clearly in the electron-density map (up to 10σ for the phosphates in the $2F_o - F_c$ map), with average B values of 18.9, 33.2 and 22.8 Å^2 in the case of the ADP, the ADP and the Mg^{2+} and ATP complexes, respectively. The highly conserved Tyr599 in the A-loop flips over from the apo structure to undergo π–π stacking with the adenine (Fig. 4). The movement of Tyr599 results in a reorientation of Thr606 and the surrounding backbone atoms of Glu604 and Leu606, breaking hydrogen bonds between β-strands β_1 and β_2, which are therefore shortened. The adenine is further stabilized by Tyr640 *via* van der Waals interactions between Tyr640 OH and N6 of the adenine (the distances between Tyr640 OH and N6 of the adenine were 3.8, 3.7 and 3.5 Å for the ADP, the ADP and the Mg^{2+} and ATP complexes, respectively; Fig. 4).

The nucleotide is also fixed by hydrogen bonds between the β-phosphate moiety, the amides of the backbones of the the Walker A residues (Gly626–Lys629) and Lys629 NZ. Additional hydrogen bonds are formed between Ser630 (backbone and OG) and the β-phosphate moiety and between Thr631 (backbone and OG1) and the α-phosphate moiety. In the ATP complex, Arg634 forms a hydrogen bond to the β-phosphate group (2.6 Å), in contrast to the ADP and the ADP plus Mg^{2+} complexes. In both these complexes Arg634 adopts another orientation, allowing van der Waals interactions with N7 of the adenine (3.9 and 3.8 Å, respectively) and the α-phosphate group (3.9 and 4.0 Å, respectively). The Mg^{2+} ion in the ADP plus Mg^{2+} complex is coordinated by the γ-phosphate group and four water molecules, whereas the sixth coordination site is occupied by Glu562 of a symmetry-related monomer (the crystal contact described in §3.2; Fig. 4*b*). The r.m.s.d. for residues Phe597–Ala601 and Glu604–Leu606 (backbone atoms) between the ATP and the ADP complexes is 1.62 Å, in contrast to 0.39 Å for a comparison of the ADP and Mg^{2+} complex with the ADP complex, indicating differences in the nucleotide-binding region between the structures obtained by soaking and cocrystallization.

The crystal structures of ABCB6 NBD extend the insights gained by triple-resonance NMR experiments and homology-modelling studies on ABCB6 NBD (Kurashima-Ito *et al.*, 2006). The structures determined in the present study clearly show how nucleotide binding results in a rearrangement of important residues within the A-loop and the Walker A motif, which are stabilized upon nucleotide binding.

3.4. The active site

Two different mechanisms have been proposed to form the basis of the catalytic mechanism within NBDs. A general base catalytic mechanism, in which a glutamic acid equivalent to Glu752 serves as a catalytic carboxylate, activating a nearby water, has been suggested for the NBDs of the ABC transporters MJ0796 and MJ1267 (Moody *et al.*, 2002). In contrast, mutational and structural studies on HlyB suggested

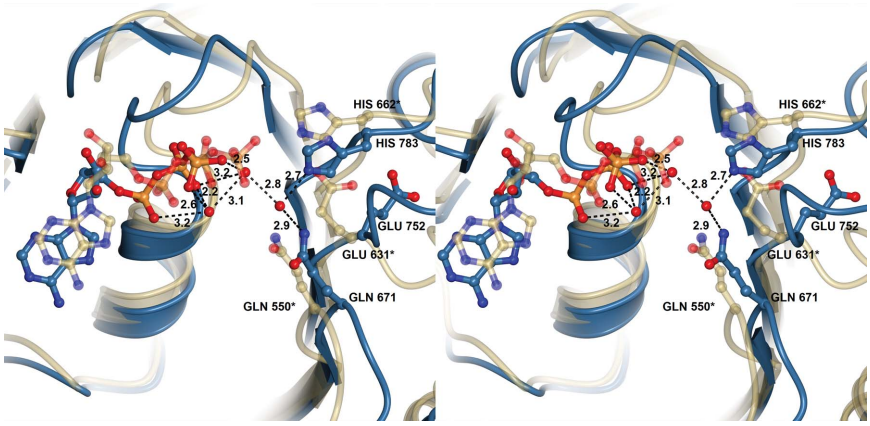

Figure 5
Comparison of the active site of ABCB6 NBD with the NBD of HlyB. The ABCB6 NBD–ATP complex is coloured blue and HlyB in complex with ATP [modelled by superimposing PDB entries 2fgj on 2fgk using the *DaliLite* server (Holm & Park, 2000); the backbone of 2fgk is shown] is coloured yellow. Important residues are shown in ball-and-stick representation and are labelled (residues of HlyB are indicated by asterisks). Water molecules are shown as red spheres for ABCB6 NBD only. This stereo figure was prepared with *CCP*4*MG* (Potterton *et al.*, 2004).

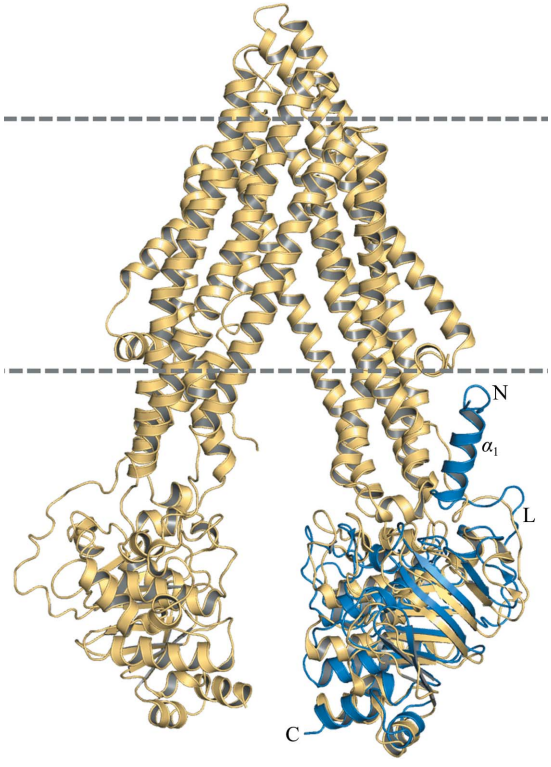

Figure 6
Superposition of ABCB6 NBD on murine P-glycoprotein. The NBD of ABCB6 in the apo form (present study), coloured blue, was superimposed on P-glycoprotein (*M. musculus*; PDB entry 3g5u), coloured yellow, with the *DaliLite* server (Holm & Park, 2000; *Z* score 30.2; r.m.s.d. 5.3 Å; sequence identity 43%). The loop connecting helix α_1 to lobe I is indicated by L. Grey dotted lines represent the cell membrane. This figure was prepared with *PyMOL* (DeLano, 2008).

substrate-assisted catalysis (SAC; Zaitseva, Jenewein, Wiedenmann *et al.*, 2005).

Since an HlyB–ATP complex could only be observed by mutating either His662 to alanine (PDB entry 2fgj; Zaitseva *et al.*, 2006) or Glu631 to glutamine (PDB entry 2fgk; Zaitseva *et al.*, 2006), these two structures were superimposed using the *DaliLite* server (*Z* score 36.3; r.m.s.d. 1.1 Å; Holm & Park, 2000) to allow a structural comparison with the ATP complex of ABCB6 NBD. Residues of HlyB are indicated with an asterisk in the following section.

The ATP complex of ABCB6 NBD has a similar orientation of the important residues in the active site compared with that of HlyB. His783 and His662* as well as Gln671 and Gln550* are orientated similarly (Fig. 5). However, His662* forms a hydrogen bond to the γ-phosphate group of the ATP* (2.7 Å; not shown in Fig. 5 for clarity), whereas the distance between the same atoms is too great in ABCB6 NBD (5.5 Å). Glu631* and Glu752 show different orientations, with Glu752 pointing away from the ATP and therefore adopting a nonproductive conformation with respect to a general base catalysis mechanism. None of the waters near the ATP can be activated by His783 or Glu752 to nucleophilically attack the ATP. Mutations of the Glu near the Walker B motif (Glu752 in ABCB6) have been shown to abrogate ATP hydrolysis in isolated NBDs of MJ0796 and MJ1267 (Moody *et al.*, 2002). Nevertheless, this Glu in HlyB was shown to act not as a catalytic base but as a platform, providing the proper orientation of the side chains in the active site (Hanekop *et al.*, 2006) that are necessary for the correct positioning of water molecules near the ATP for SAC.

The observations described and discussed above favour a substrate-assisted catalysis mechanism over a general base catalysis mechanism during ATP hydrolysis in ABCB6 NBD. However, the catalytically important Mg^{2+} ion is absent from the present ABCB6 NBD–ATP complex and would recruit an additional water molecule to the active site that could influence the orientations of side chains and the catalytic mechanism, as could a dimerization during the catalytic cycle.

3.5. Comparison with other NBDs

The two-lobe structure of NBDs is highly conserved in all known structures of ABC transporters and their isolated NBDs. The superposition of different NBDs on ABCB6 NBD shows low r.m.s.d.s of about 2.4 Å, with a sequence identity of between 24% and 40% (Supplementary Fig. S2). Lobe I superimposes with lower differences, whereas lobe II/the ABC α subdomain is more structurally diverse. The most significant differences between the known structures are at the C- and N-termini. In comparison with other known structures of isolated NBDs, ABCB6 NBD in the present study also reveals part of the loop and helix α_1 connecting the NBD to the TMDs of full-length ABCB6 (Fig. 6). However, since the loop connecting α_1 to lobe I is highly flexible, movements of α_1 might also prevent nucleotide-dependent dimerization of the

isolated NBD of ABCB6 by blocking the monomer–monomer interface.

4. Conclusions

The overall structure of the NBD of human ABCB6 is similar to other reported NBD structures. However, insights into a possible catalytic mechanism for ATP hydrolysis and insights into the region connecting both TMDs and NBDs in ABCB6 could be obtained. Since ABCB6 fulfils an important role in haem biosynthesis, it would be interesting to find out whether mutations in ABCB6 and its NBD correlate with diseases of mitochondrial dysfunction.

This work was supported by various grants from the Deutsche Forschungsgemeinschaft and the Fonds der Chemischen Industrie to DJ and DWH. The authors greatly acknowledge beamtime and beamline support at DESY (Hamburg) and ESRF (Grenoble). MH thanks Roman Fedorov for data collection at ESRF.

References

Aller, S. G., Yu, J., Ward, A., Wenig, Y., Chittaboina, S., Zhuo, R., Harrell, P. M., Trinh, Y. T., Zhang, Q., Urbatsch, I. L. & Chang, G. (2009). *Science*, **323**, 1718–1722.
Allikmets, R. *et al.* (1997). *Nature Genet.* **15**, 236–246.
Atwell, S., Conners, K., Emtage, S., Gheyi, T., Lewis, H., Lu, F., Romero, R. & Zhao, X. (2007). *Pediatr. Pulmonol. Suppl.* **30**, 100–101.
Berge, K. E., Tian, H., Graf, G. A., Yu, L., Grishin, N. V., Schultz, J., Kwiterovich, P., Shan, B., Barnes, R. & Hobbs, H. H. (2000). *Science*, **290**, 1771–1775.
Bernstein, F. C., Koetzle, T. F., Wiliams, G. J. B., Meyer, E. F. Jr, Brice, M. D., Rogers, J. R., Kennard, O., Shimanouchi, T. & Tasumi, M. (1977). *J. Mol. Biol.* **112**, 535–542.
Borst, P. & Elferink, R. O. (2002). *Annu. Rev. Biochem.* **71**, 537–592.
Chen, J., Lu, G., Lin, J., Davidson, A. L. & Quiocho, F. A. (2003). *Mol. Cell*, **12**, 651–661.
Dawson, R. J., Hollenstein, K. & Locher, K. P. (2007). *Mol. Microbiol.* **65**, 250–257.
Dean, M., Rzhetsky, A. & Allikmets, R. (2001). *Genome Res.* **11**, 1156–1166.
Dean, M., White, M. B., Amos, J., Gerrard, B., Stewart, C., Khaw, K. T. & Leppert, M. (1990). *Cell*, **61**, 863–870.
DeLano, W. L. (2008). *The PyMOL Molecular Viewer.* DeLano Scientific, Palo Alto, Calilfornia, USA.
Diederichs, K., Diez, J., Greller, G., Muller, C., Breed, J., Schnell, C., Vonrhein, C., Boos, W. & Welte, W. (2000). *EMBO J.* **19**, 5951–5961.
Emadi-Konjin, H. P., Zhang, H., Anandan, V., Sun, D., Schuetz, J. & Furuya, K. N. (2002). *Biochim. Biophys. Acta*, **1574**, 117–130.
Emsley, P., Lohkamp, B., Scott, W. G. & Cowtan, K. (2010). *Acta Cryst.* D**66**, 486–501.
Gaudet, R. & Wiley, D. C. (2001). *EMBO J.* **20**, 4964–4972.
Gouet, P., Courcelle, E., Stuart, D. I. & Métoz, F. (1999). *Bioinformatics*, **15**, 305–308.
Guo, X., Harrison, R. W. & Tai, P. C. (2006). *J. Bacteriol.* **188**, 2383–2391.
Hanekop, N., Zaitseva, J., Jenewein, S., Holland, I. B. & Schmitt, L. (2006). *FEBS Lett.* **580**, 1036–1041.
Higgins, C. F. (1992). *Annu. Rev. Cell Biol.* **8**, 67–113.
Higgins, C. F. & Linton, K. J. (2004). *Nature Struct. Mol. Biol.* **11**, 918–926.
Holland, I. B. & Blight, M. A. (1999). *J. Mol. Biol.* **293**, 381–399.
Hollenstein, K., Dawson, R. J. & Locher, K. P. (2007). *Curr. Opin. Struct. Biol.* **17**, 412–418.
Holm, L. (1998). *Curr. Opin. Struct. Biol.* **8**, 372–379.
Holm, L. & Park, J. (2000). *Bioinformatics*, **16**, 566–567.
Hung, L.-W., Wang, I.-X., Nikaido, K., Liu, P.-Q., Ames, G. F. & Kim, S.-H. (1998). *Nature (London)*, **396**, 703–707.
Jones, P. M. & George, A. M. (2007). *Cell. Mol. Life Sci.* **61**, 682–699.
Kabsch, W. (2010). *Acta Cryst.* D**66**, 125–132.
Kabsch, W. & Sander, C. (1983). *Biopolymers*, **22**, 2577–2637.
Karpowich, N., Martsinkevich, O., Millen, L., Yuan, Y. R., Dai, P. L., MacVey, K., Thomas, P. J. & Hunt, J. F. (2001). *Structure*, **9**, 571–586.
Kispal, G., Csere, P., Guiard, B. & Lill, R. (1997). *FEBS Lett.* **418**, 346–350.
Kispal, G., Csere, P., Prohl, C. & Lill, R. (1999). *EMBO J.* **15**, 3981–3989.
Krishnamurthy, P. C., Du, G., Fukuda, Y., Sun, D., Sampath, J., Mercer, K. E., Wang, J., Soso-Pineda, B., Murti, K. G. & Schuetz, J. D. (2006). *Nature (London)*, **443**, 586–589.
Krissinel, E. & Henrick, K. (2007). *J. Mol. Biol.* **372**, 774–797.
Kurashima-Ito, K., Ikeya, T., Senbongi, H., Tochio, H., Mikawa, T., Shibata, T. & Ito, Y. (2006). *J. Biomol. NMR*, **35**, 53–71.
Lamzin, V. S. & Wilson, K. S. (1993). *Acta Cryst.* D**49**, 129–147.
Langer, G., Cohen, S. X., Lamzin, V. S. & Perrakis, A. (2008). *Nature Protoc.* **3**, 1171–1179.
Larkin, M. A., Blackshields, G., Brown, N. P., Chenna, R., McGettigan, P. A., McWilliam, H., Valentin, F., Wallace, I. M., Wilm, A., Lopez, R., Thompson, J. D., Gibson, T. J. & Higgins, D. G. (2007). *Bioinformatics*, **23**, 2947–2948.
Laskowski, R. A., MacArthur, M. W., Moss, D. S. & Thornton, J. M. (1993). *J. Appl. Cryst.* **26**, 283–291.
Lewis, H. A. *et al.* (2004). *EMBO J.* **23**, 282–293.
Lewis, H. A., Zhao, X., Wang, C., Sauder, J. M., Rooney, I., Noland, B. W., Lorimer, D., Kearins, M. C., Conners, K., Condon, B., Maloney, P. C., Guggino, W. B., Hunt, J. F. & Emtage, S. (2005). *J. Biol. Chem.* **280**, 1346–1353.
Martin, A. C. R. (2009). *ProFit.* http://www.bioinf.org.uk/profit.
Matthews, B. W. (1968). *J. Mol. Biol.* **33**, 491–497.
Moody, J. E., Millen, L., Binns, D., Hunt, J. F. & Thomas, P. J. (2002). *J. Biol. Chem.* **277**, 21111–21114.
Murshudov, G. N., Vagin, A. A. & Dodson, E. J. (1997). *Acta Cryst.* D**53**, 240–255.
Ose, T., Fujie, T., Yao, M., Watanabe, N. & Tanaka, I. (2004). *Proteins*, **57**, 635–638.
Oswald, C., Jenewein, S., Smits, S. H. J., Holland, I. B. & Schmitt, L. (2008). *J. Struct. Biol.* **162**, 85–93.
Painter, J. & Merritt, E. A. (2006*a*). *Acta Cryst.* D**62**, 439–450.
Painter, J. & Merritt, E. A. (2006*b*). *J. Appl. Cryst.* **39**, 109–111.
Paterson, J. K., Shukla, S., Black, C. M., Tachiwada, T., Garfield, S., Wincovitch, S., Ernst, D. N., Agadir, A., Li, X., Ambudkar, S. V., Szakacs, G., Akiyama, S. & Gottesman, M. M. (2007). *Biochemistry*, **46**, 9443–9452.
Potterton, L., McNicholas, S., Krissinel, E., Gruber, J., Cowtan, K., Emsley, P., Murshudov, G. N., Cohen, S., Perrakis, A. & Noble, M. (2004). *Acta Cryst.* D**60**, 2288–2294.
Procko, E., Ferrin-O'Connell, I., Ng, S.-L. & Gaudet, R. (2006). *Mol. Cell*, **24**, 51–62.
Ramachandran, G. N. & Sasisekharan, V. (1968). *Adv. Protein Chem.* **23**, 283–438.
Ramaen, O., Leulliot, N., Sizun, C., Ulryck, N., Pamlard, O., Lallemand, J.-Y., Van Tilbeurgh, H. & Jacquet, E. (2006). *J. Mol. Biol.* **359**, 940–949.
Scheffel, F., Demmer, U., Warkentin, E., Schneider, E. & Ermler, U. (2005). *FEBS Lett.* **579**, 2953–2958.

Schmitt, L., Benabdelhak, H., Blight, M. A., Holland, I. B. & Stubbs, M. T. (2003). *J. Mol. Biol.* **330**, 333–342.
Schneider, E. & Hunke, S. (1998). *FEMS Microbiol. Rev.* **22**, 1–20.
Sharom, F. J. (2008). *Pharmacogenomics*, **9**, 105–127.
Smith, P. C., Karpowich, N., Millen, L., Moody, J. E., Rosen, J., Thomas, P. J. & Hunt, J. F. (2002). *Mol. Cell*, **10**, 139–149.
Szakacs, G., Annereau, J. P., Lababidi, S., Shankavaram, U., Arciello, A., Bussey, K. J., Reinhold, W., Guo, Y., Kruh, G. D., Reimers, M., Weinstein, J. N. & Gottesman, M. M. (2004). *Cancer Cell*, **6**, 129–137.
Thibodeau, P. H., Brautigam, C. A., Machius, M. & Thomas, P. J. (2005). *Nature Struct. Mol. Biol.* **12**, 10–16.
Tsuchida, M., Emi, Y., Kida, Y. & Sakaguchi, M. (2008). *Biochem. Biophys. Res. Commun.* **369**, 369–375.
Vagin, A. & Teplyakov, A. (2000). *Acta Cryst.* D**56**, 1622–1624.
Vedadi, M. *et al.* (2007). *Mol. Biochem. Parasitol.* **151**, 100–110.
Verdon, G., Albers, S. V., Dijkstra, B. W., Driessen, A. J. & Thunnissen, A. M. (2003). *J. Mol. Biol.* **330**, 343–358.
Vree, J. M. de, Jacquemin, E., Sturm, E., Cresteil, D., Bosma, P. J., Aten, J., Deleuze, J. F., Desrochers, M., Burdelski, M., Bernard, O., Elferink, R. O. & Hadchouel, M. (1998). *Proc. Natl Acad. Sci. USA*, **95**, 282–287.
Vriend, G. (1990). *J. Mol. Graph.* **8**, 52–56.
Wada, M., Toh, S., Taniguchi, K., Nakamura, T., Uchiumi, T., Kohno, K., Yoshida, I., Kimura, A., Sakisaka, S., Adachi, Y. & Kuwano, M. (1998). *Hum. Mol. Genet.* **7**, 203–207.
Yuan, Y.-R., Blecker, S., Martsinkevich, O., Millen, L., Thomas, P. J. & Hunt, J. F. (2001). *J. Biol. Chem.* **276**, 32313–32321.
Zaitseva, J., Jenewein, S., Jumpertz, T., Holland, I. B. & Schmitt, L. (2005). *EMBO J.* **24**, 1901–1910.
Zaitseva, J., Jenewein, S., Wiedenmann, A., Benabdelhak, H., Holland, I. B. & Schmitt, L. (2005). *Biochemistry*, **44**, 9680–9690.
Zaitseva, J., Oswald, C., Jumpertz, T., Jenewein, S., Wiedenmann, A., Holland, I. B. & Schmitt, L. (2006). *EMBO J.* **25**, 3432–3443.